Identification of periodic bursts in surface EMG: Applications to the erector spinae muscles of sitting violin players

Elsevier Editorial System(tm) for Biomedical Signal Processing and Control

Manuscript Draft

Manuscript Number:

Title: Identification of periodic bursts in surface EMG: applications to the erector spinae muscles of sitting violin players.

Article Type: Research Paper

Keywords: surface electromyography; sEMG, burst detection; burst frequency; intermittent posture control; high density sEMG

Corresponding Author: Professor Roberto Merletti,

Corresponding Author's Institution: Politecnico di Torino

First Author: Amir Khorrami Chokami, PhD

Order of Authors: Amir Khorrami Chokami, PhD; Mauro Gasparini; Roberto Merletti

Abstract: Abstract

Objective. This work compares two known and one novel techniques for the detection of surface EMG (sEMG) quasi-periodic burst-like signals and estimation of their frequency. Two methods use a fixed (FT) or automatically selected threshold (OT) and the third (ES) is based on the spectral analysis of the envelope signal.
Methods. The methods are compared using both simulated signals and samples of High Density sEMG experimental signals collected using electrode arrays applied to the erector spinae muscles of sitting violinists.
Results. The ES method requires only one parameter, detects presence /absence of bursts and their frequency, even in cases of a few missing bursts. It does not provide their duration. The FT method requires the selection of a fixed threshold value and two parameters, estimates burst duration but is applicable only if bursts are present. The OT method identifies an optimal threshold, requires two parameters, estimates burst duration but behaves irregularly when bursts are small or absent.
Conclusions. The ES method provides the estimates closest to those of an expert human counter and is not sensitive to amplitude fluctuations. It is suitable when the general bursts "periodicity" is of interest but does not provide an exact count. The FT and OT methods are sensitive to amplitude fluctuations and identify random threshold crossings as bursts even when burst activity is absent.
Significance. Postural muscles are often activated in a burst-like fashion. Determining the frequency and duty cycle of the bursts is important for studying the neuro-physiological mechanism generating them.

Cover letter

Torino, May 25 2020

Dear Editor-in-Chief of BSPC: Dr. Panicos A. Kyriacou ,

On behalf of all authors I respectfully submit to Biomedical signal processing and control the following article

Identification of periodic bursts in surface EMG: applications to the erector spinae muscles of sitting violin players.

A. Khorrami Chokami [1], M. Gasparini [2], R. Merletti [3*]
[1] Depart. ESOMAS, University of Turin, Torino, Italy, amir.khorramichokami@unito.it
[2] Depart. of Mathematical Sciences, Politecnico di Torino, Torino, Italy, mauro.gasparini@polito.it
[3] LISiN, Depart. of Electronics and Telecommunications Politecnico di Torino, Torino, Italy
* (corresponding author) roberto.merletti@formerfaculty.polito.it

This paper has not been submitted to other Journals.

Credit author statement:

RM : conceptualization and writing original draft
AKC: Data Curation, Application of statistical, mathematical, computational techniques to analyze or synthesize study data
MG : Statistical consultation, draft revision,

Declaration of interests

☒ The authors declare that they have no known competing financial interests or personal relationships that could have appeared to influence the work reported in this paper.

I look forward to receiving comments from the reviewers.

Best regards

Roberto Merletti
On behalf of A. Khorrami Chokami and M. Gasparini.

Identification of periodic bursts in surface EMG: applications to the erector spinae muscles of sitting violin players.

A. Khorrami Chokami [1], M. Gasparini [2], R. Merletti [3*]

[1] Depart. ESOMAS, University of Turin, Torino, Italy, amir.khorramichokami@unito.it
[2] Depart. of Mathematical Sciences, Politecnico di Torino, Torino, Italy, mauro.gasparini@polito.it
[3] LISiN, Depart. of Electronics and Telecommunications Politecnico di Torino, Torino, Italy
* (corresponding author) roberto.merletti@formerfaculty.polito.it

Abstract (248 words out of 250 words allowed)

Objective. This work compares two known and one novel techniques for the detection of surface EMG (sEMG) quasi-periodic burst-like signals and estimation of their frequency. Two methods use a fixed (FT) or automatically selected threshold (OT) and the third (ES) is based on the spectral analysis of the envelope signal.
Methods. The methods are compared using both simulated signals and samples of High Density sEMG experimental signals collected using electrode arrays applied to the erector spinae muscles of sitting violinists.
Results. The ES method requires only one parameter, detects presence /absence of bursts and their frequency, even in cases of a few missing bursts. It does not provide their duration. The FT method requires the selection of a fixed threshold value and two parameters, estimates burst duration but is applicable only if bursts are present. The OT method identifies an optimal threshold, requires two parameters, estimates burst duration but behaves irregularly when bursts are small or absent.
Conclusions. The ES method provides the estimates closest to those of an expert human counter and is not sensitive to amplitude fluctuations. It is suitable when the general bursts "periodicity" is of interest but does not provide an exact count. The FT and OT methods are sensitive to amplitude fluctuations and identify random threshold crossings as bursts even when burst activity is absent.
Significance. Postural muscles are often activated in a burst-like fashion. Determining the frequency and duty cycle of the bursts is important for studying the neurophysiological mechanism generating them.

Keywords: surface electromyography**,** sEMG, burst detection, burst frequency, intermittent posture control, high density sEMG.

Funding: This research did not receive any specific grant from funding agencies in the public, commercial, or not-for-profit sectors.

Conflict of interest. The authors declare no conflict of interest.

Acknowledgment.
The authors are grateful to A. Russo, S. D'Emanuele, F. Serafino, and A, Aranceta-Garza for collecting the signals from which the samples used in this work have been taken.

1. Introduction

Surface electromyography (sEMG) is widely used for the study and measurement of muscle activity. The sEMG signal detected by electrodes applied to the skin above the muscle(s) of interest is the algebraic summation of the contributions of the individual motor units (MU) forming the muscle. A MU is a bundle of muscle fibers innervated by a single motor neuron and, therefore, activated synchronously by each discharge of the motor neuron. Each motor neuron discharge triggers a MU action potential (MUAP) propagating from the neuro-muscular junction to the fiber-tendon junctions at the two fiber ends. The algebraic sum of the surface contributions of the MUAPs is the sEMG signal. During a constant-force isometric contraction, the discharge rate of each MU is approximately constant (within the range of 8-30 discharges/s depending on the effort) and out of synch with respect to the others so that the summation has an approximately Gaussian probability density function (pdf) when at least a few dozens of MU are activated [Merletti2016].

Posture control (quiet standing, sitting, etc) can be modeled like an inverted pendulum. When facing this balancing task, the CNS often adopts an intermittent control strategy, that is, the system modulates the activation of a muscle or a group of muscles. This phenomenon has been extensively investigated [Vieira2012, Gross 2002, Tanabe2017, Morasso 2011, Gawthtrop 2011]. The intermittency of this control has been observed as sEMG "bursts" in the activation of the gastrocnemius, at the rate about 2 bursts/s during quiet standing [Vieira 2012], and in the right and left erector spine in sitting violinists, at the rate of about 2.4-3.1 bursts/s [Russo 2019]. The most common methods for burst detection are based on the analysis of the signal "envelope". A very extensive literature exists on the envelope-based analysis of muscle activation intervals [Guerrero2014, Guerrero2019, Bonato1998, Xu2013, Ranaldi2018, Tenan2017, Yang2017, Jubany2016, Ozgunen2010, Allison2003].

The purpose of this work is to compare two known and one novel techniques for detection of sEMG bursts and estimation of their frequency. This is achieved using both simulated signals and samples of High Density sEMG (HDsEMG) experimental signals collected, in a previous work, from the erector spinae of a sitting violinist [Russo 2019]. Two methods use a fixed or automatically selected threshold whereas the third is based on the spectral analysis of the envelope signal.

2. Methods: Experimental protocols and signal acquisition.

The problem of sEMG burst analysis can be broken down into a) signal conditioning and envelope estimation, described in Section 2.2, b) burst detection, described in Section 2.3, and c) estimation of burst properties. This work is focused on the estimation of burst frequency.

2.1 Experimental protocol and signal acquisition.

Experimental signals available from previous work on sitting violinists [Russo 2019] have been used. In summary, these signals had been collected using the HDsEMG technique that provides "images" of the monopolar evolving instantaneous sEMG potential distribution. Two electrode grids, each of 16 rows and 8 columns, had been placed on the right and left lumbar erector spinae of nine sitting violinists as indicated in Fig.1a. The grids (Fig. 1b) had electrode size and inter-electrode distance satisfying the spatial sampling conditions described in [Merletti2019]. The violinists played for two hours without breaks and the sEMG signals were acquired every 5 minutes for 20s. The same piece of music was played during each of these 20 s recordings.

In this work, one representative example of 20-s recording will be considered at the beginning of the task, consisting of two sets of signals from the right and the left electrode array placed on one subject. Similar results were obtained from other sets of signals from the nine subjects and will be reported elsewhere.

Sixteen monopolar signals were recorded from each column, amplified and band-pass filtered at 20 Hz and 500 Hz (analog antialiasing filter), sampled at 2048 sample/s and A/D converted (16 bits) with a resolution of 0.5 μV. See [Russo 2019] for further details. Fifteen longitudinal single differential (SD or bipolar) signals where obtained from each column for a total of 120 channels from each of the two arrays.

The erector spinae is a muscle group formed by the spinalis, iliocostalis and longissimus lumborum, whose approximate fiber direction is indicated in Fig 1a [DeFoa1989]. Because of the propagation of action potentials along the muscle fibers a high degree of correlation is observed between signals of the same column (see Fig.2 in [Russo2019]). Burst correlation/synchronization is observed in Fig. 1c between the two sides. Lower signal amplitudes are expected in caudal and lateral parts of the arrays because electrodes are on the tendons or away from the muscles, respectively.

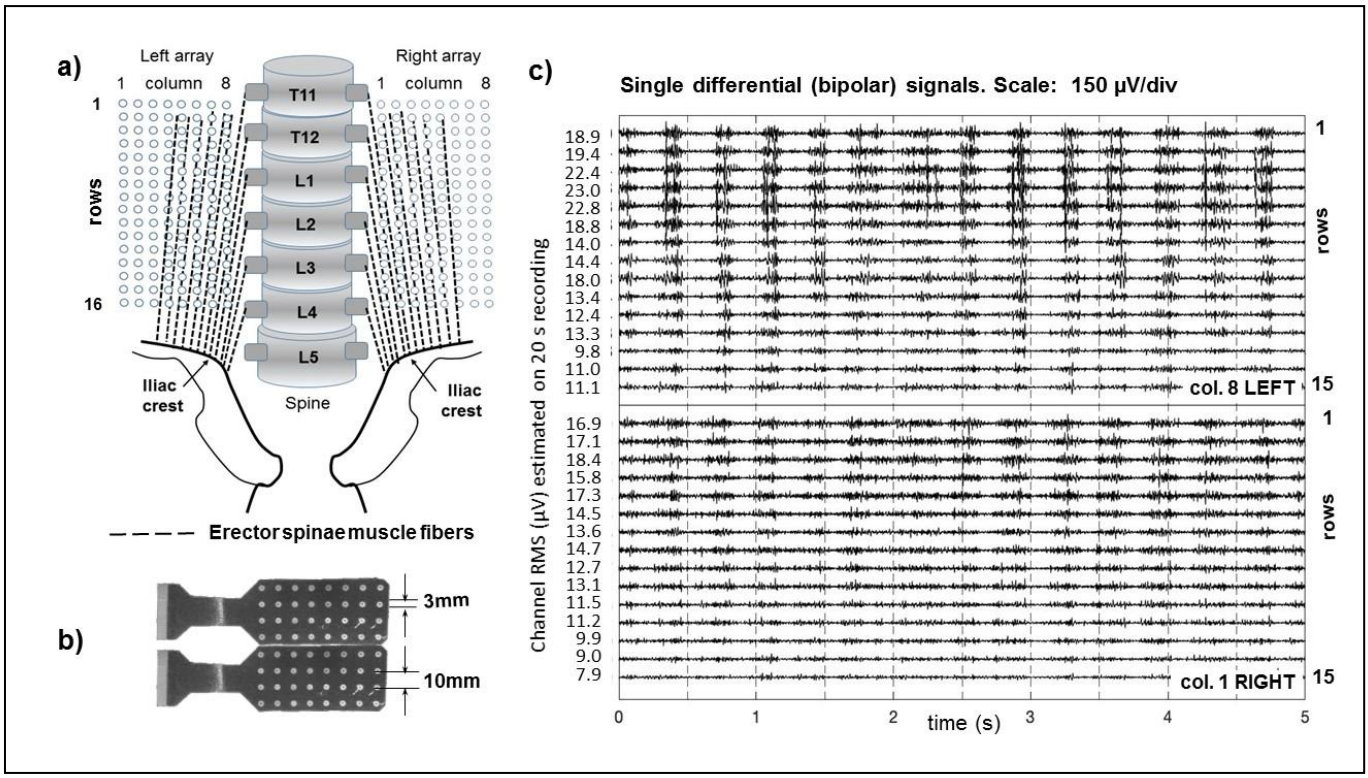

Fig. 1. Surface EMG signal: single differential signals along each column of a grid of 16x8 electrodes (15x8 differential channels). a) position of the electrode grids on the lumbar erector spinae, b) electrode grids: two such grids, one proximal and one distal, were placed on each side (128 electrodes on each side). c) 5s long signal recording from col 7 (left) and col. 2 (right) of subject LS. The numbers on the left of each trace indicate the RMS value of each channel computed over the 20 s duration of the recording. Larger signals are detected in the rostral-medial parts of the arrays. Bursts are evident and are synchronized along each column, across columns and in the left and right side.

2.2. Signal conditioning, removal of power line interference.

The digital signals were filtered again between 20 Hz and 400 Hz to limit noise. Since the substantially isometric effort performed by the erector spinae is moderate, the sEMG amplitude is small (Fig. 1c) and the interference from the power line (50 Hz) is relevant. Such interference is evident from the spectrum of each sEMG channel as a series of peaks at 50 Hz and its first 3-4 harmonics. This interference was eliminated using the "spectral interpolation" method proposed by [Mewett2004] and used by [Leske2019, Russo 2019].

2.3. Burst detection methods.

The simplest and most widely used procedure for envelope estimation implies taking the absolute value of the raw signal, apply a moving average window (MAW), or a bidirectional (non causal) low-pass filter, to smooth the result and obtain the envelope. Subsequent application of a threshold

(Th) will produce a binary signal indicating if the muscle is active (envelope above threshold) or not (envelope below threshold). Post-processing algorithms are usually required to remove isolated short "spurious" 1s or 0s whose duration is indicated as "tolerance" (TOL)). These choices introduce some degree of arbitrariness that can be reduced by testing the algorithms with simulated signals and empirically selecting the MAW, Th, and TOL values leading to the smallest burst counting error (Section 3). The "gold standard" count is known in simulations and provided by an expert Human Counter (HC) in the case of experimental signals. The behavior of these methods in the case of no bursts is not discussed in the literature proposing them.

3. Methods: Testing burst detection algorithms with simulated signals

3.1. Simulated signals

Computer simulated signals were used for the purpose of testing and comparing burst detection algorithms applied to single sEMG channels. Single channel signals, such as those depicted in Fig 1c, were simulated as the sum of two components: background noise (and possibly some sEMG) and burst sEMG signal. The background noise is mostly due to the electrode-skin interface and to the electronics and is generally assumed to have a Gaussian distribution. At low contraction levels the sEMG has a distribution between Laplacian and Gaussian [Nazarpour2013]. Simulated signals were computer generated, for the duration of 20 s and sampling frequency of 2048 Hz (40960 samples) using Matlab 10. Each channel of sEMG was simulated as:

$$Y(t) = X_0(t) + z(t) * X_1(t) \quad (1)$$

Where $X_0(t)$ and $X_1(t)$ are two zero-mean Gaussian processes with standard deviation σ_0 and σ_1, filtered by a 4th order non-causal Butterworth bandpass filter with cut-off frequencies of 20 Hz and 400 Hz, $z(t)$ is a train of Gaussian impulses having frequency of 2.5 bursts/s (50 bursts in 20s) and standard deviation σ_z = 54 ms, used to amplitude modulate $X_1(t)$ and generate bursts similar to those observed experimentally (Fig. 3). The burst duration is $\pm 2\sigma_z$, that is about 216 ms. $X_0(t)$ has fixed σ_0 =1 and $X_1(t)$ has variable σ_1, simulating weak to strong burst amplitudes. The case of no bursts is simulated using normally distributed signals with zero mean and unit variance ($X_0(t)$).

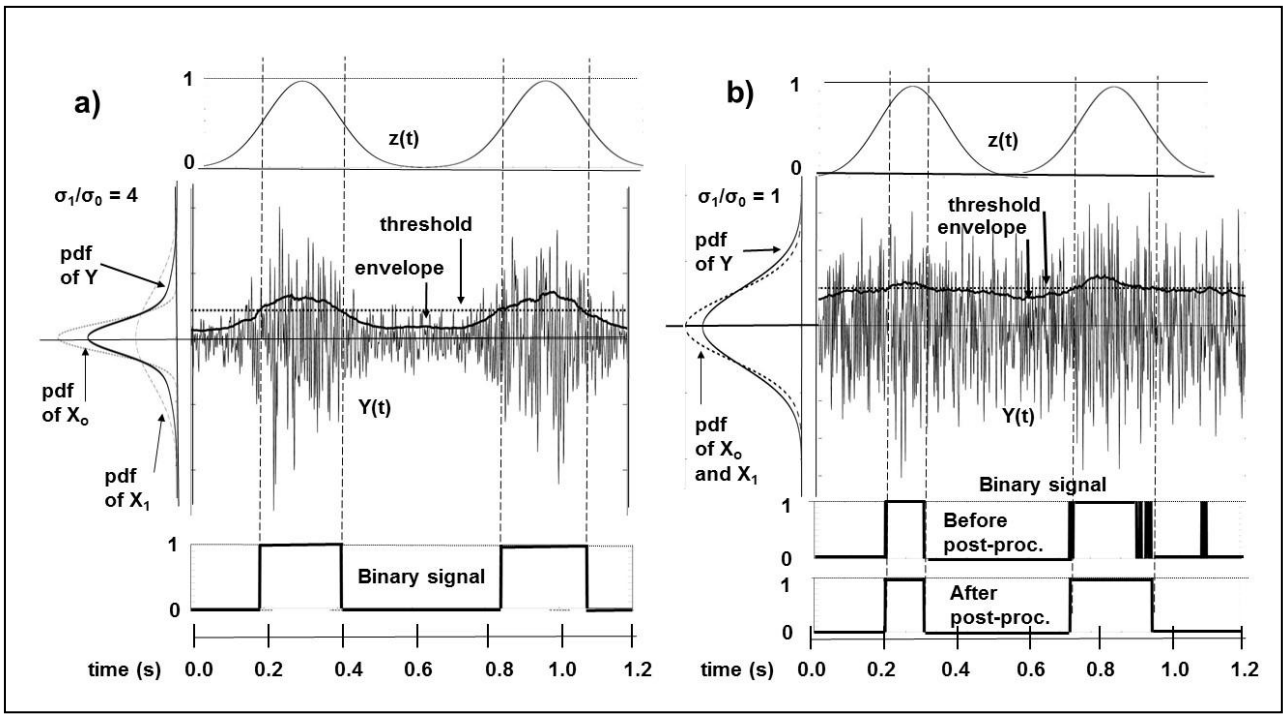

Fig. 2. Simulated sEMG signals obtained as indicated in eq. 1. a) $\sigma_1/\sigma_0 = 4$ (strong bursts), b) $\sigma_1/\sigma_0 = 1$ (weak bursts). Top panels: signal z(t) modulating $X_1(t)$. Mid panels: simulated burst signals with their probability density functions and detected envelope (rectified values of Y(t) smoothed with a 80 ms wide moving average window). Lower panels: binary signal resulting from the application of a threshold to the envelope, before and after post-processing with a tolerance of 50 ms.

180 The upper panels in Fig. 2 show examples of simulated signals used to test the algorithms described in Section 3.2. Fig. 3 compares a 2-s segment of an experimental signal with a simulated signal with $\sigma_1/\sigma_0 = 4$.

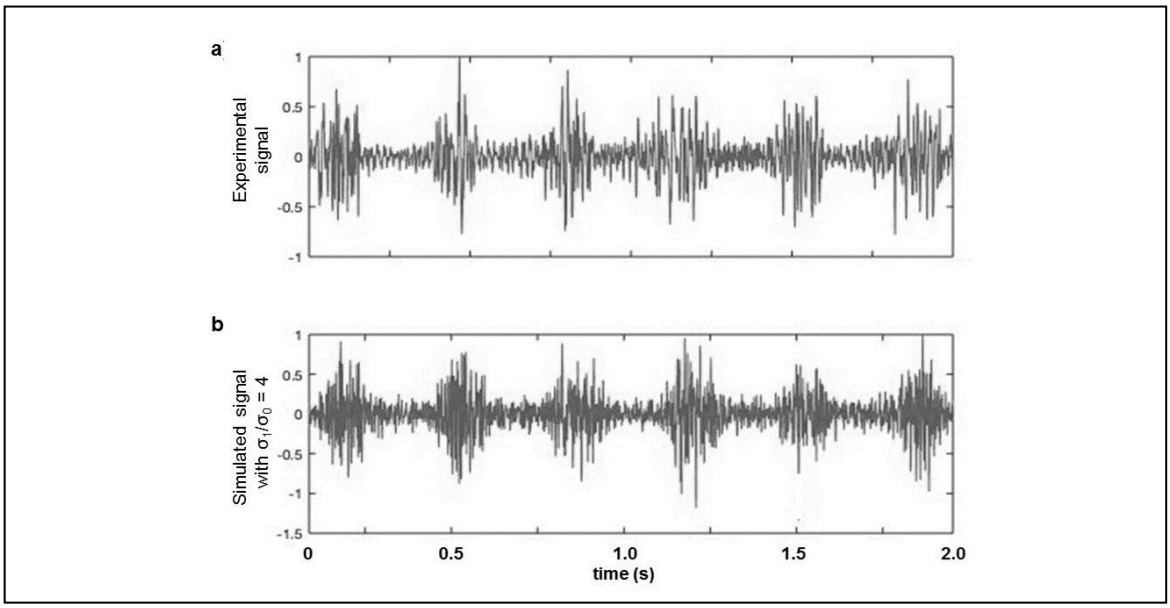

Fig. 3. Example of experimental (a) and simulated (b) single channel signals showing clear bursts. Each signal is normalized to its positive peak value.

3.2. Burst detection algorithms

Three different approaches for burst detection have been tested in this work. The signal structure described in Section 3.1 (eq. 1 and Fig. 2) was used to compare the three methods using a sequence of Gaussian bursts with σ = 54 ms for z(t) which provides a good match with experimental bursts (Fig. 3). A set of one hundred signal realizations were used to obtain boxplots of the estimated burst frequency for each method and each set of simulation parameters, so that the optimal set of parameters could be identified. All three approaches operate on the envelope signal (mid panels of Fig. 2). The envelope was obtained by applying a moving average window filter (MAW) to |Y(t)| and then removing the mean (DC component) and slow random fluctuations by means of a high pass bidirectional (non causal) 4^{th} order Butterworth filter with cut-off at 0.5 Hz. The MAW was tested in the range 60 ms to 100 ms, based on the approximate experimentally observed burst duration (150-250 ms) indicated in previous work [Russo 2019] as well as by visual observation. The window was shifted one sample at a time. Fig 4 shows examples of simulated Y(t) signals obtained for five values of σ_1/σ_0 and Gaussian pulse modulation.

The first method is based on the Envelope Spectrum (ES) and is suitable for quasi-periodic bursts. It is based on the analysis of the power spectral density (PSD) of the envelope of the rectified signal. This approach is used to extract the burst rate as identified by the largest frequency component of the PSD in the 1-5 Hz bandwidth.

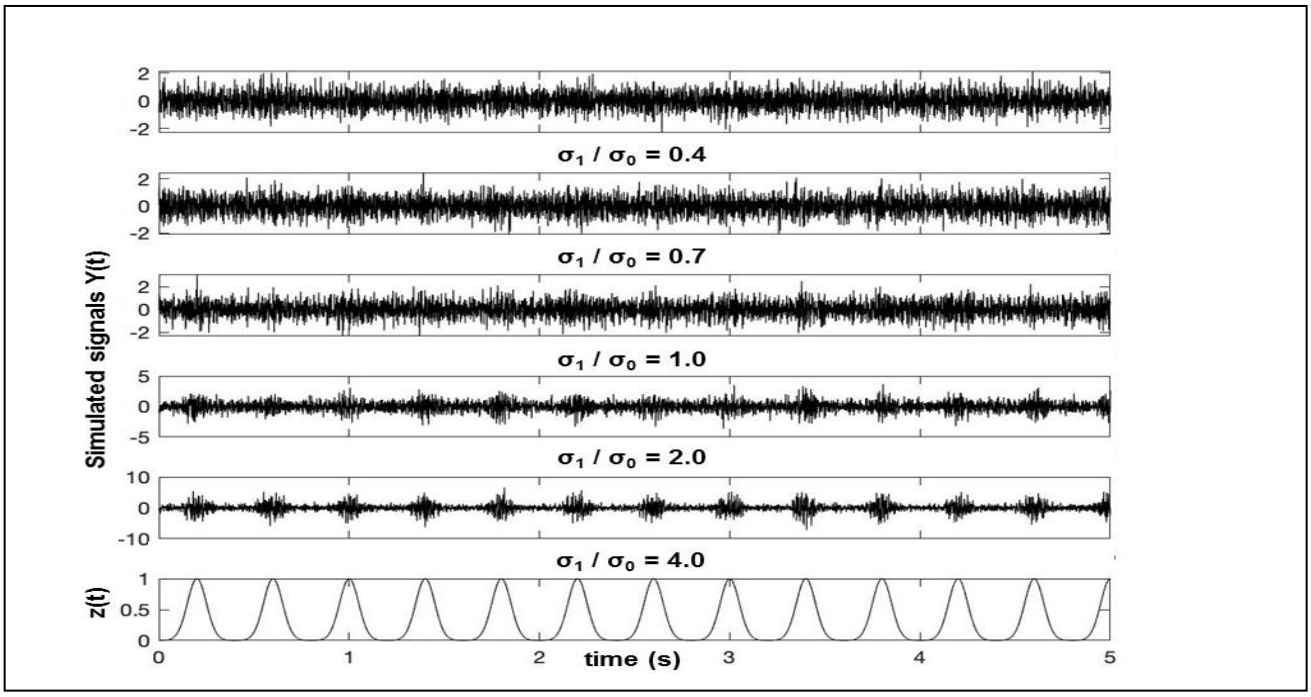

Fig. 4. Examples of simulated Y(t) signals modulated with a Gaussian pulse train and five ratios of σ_1/σ_0 (eq. 1). The burst frequency is 2.5 bursts/s and can be visually detected by an expert human assessor for $\sigma_1/\sigma_0 > 0.7$.

The second method tested is based on the empirical selection of a Fixed Threshold value based on testing with simulated signals (Section 3.2.2) and is referred to as FT. The third method is based on the statistical analysis of the signal, to obtain an "Optimal" Threshold value using a Bayesian approach, as proposed by Guerrero et al. [Guerrero2014, Guerrero2019] and is referred to as OT. All three methods require the definition of "optimal" parameters that are estimated from simulated signals and verified in experimental signals against counts provided by the HC "gold standard".

3.2.1. Method ES. Burst counting by spectral analysis of the signal envelope.

The method operates on the power spectral density (PSD) of the envelope of each simulated or experimental SD conditioned signal and is based on the inspection of the peak of the PSD. For each 20 s recording, the PSD of the envelope is computed by means of the Welch periodogram on nine time windows of 4 s each, with 50% overlapping and zero padding to 8 s (resulting in a spacing between spectral lines = 0.125 Hz). If a "sharp isolated peak" is identified in the frequency range 1-5 Hz, bursts are defined as present at the peak's frequency. To recognize a "sharp isolated peak" three conditions must be satisfied after the largest spectral line of the PSD of the envelope signal is identified: 1) no more than three adjacent spectral lines above 80% of the peak, b) no more than three additional adjacent spectral lines between 50% and 80% of the peak,

and c) all other spectral lines (within 1-5 Hz) below 50% of the peak. If these three conditions are satisfied, the frequency of the peak is taken as the burst frequency, otherwise, no bursts are detected. These conditions were identified, after extensive testing on simulated and experimental signals and comparison with visual burst counts by a human expert. They can be modified to "tune" the algorithm sensitivity to bursts.

3.2.2. Method FT. Burst counting based on fixed threshold value.

A threshold (Th) is set at a specified quantile of the distribution of the envelope signal (Fig. 2). A "tolerance" (TOL) is set in the post-processing to eliminate spurious 1s and 0s of duration lower than TOL (bottom plots of Fig. 2b). A number of algorithms have been proposed to eliminate these uncertainties by post processing [Bonato1998, Yang2017].

Based on these works interval tolerances in the range of 30-50 ms were tested and did not appear to be very critical. A value TOL = 50 ms was selected.

3.2.3. Method OT. Burst counting based on an optimal threshold value.

This burst detection algorithm is described by Guerrero et al. [Guerrero2019], and is shortly summarized in the Appendix. It assumes that the signal consists of a mixture of two Gaussian components. When $\sigma_1 << \sigma_0$, or $\sigma_1 = 0$, the starting assumption no longer holds, the two Gaussian components cannot be identified and the algorithm finds a high threshold (no longer meaningful) resulting in a burst count very low or null, as expected. Both methods FT and OT require a TOL parameter and provide information about the burst duration while method ES provides only the "dominant" burst frequency.

4. Methods: Burst detection and counting in experimental signals

After selecting the values of Th, MAW, TOL suggested by simulations, the three algorithms described in Section 3 were applied to experimental signals selected among those collected in previous work [Russo2019] (see Section 2). One 20-s array recording from the right side and one from the left side were used as an application example. Since not all channels of a grid present burst-like sEMG signals (Fig. 1c) a criterion must be defined to indicate presence or absence, and frequency of the bursts. As discussed in Sections 5 and 6, the three algorithms behave differently with respect to both presence/absence of bursts and amplitude regularity. A criterion for deciding about the global presence/absence of bursts and their frequency in the muscle(s) under a grid (or a portion of it) could be based on the definition of a sufficiently large "region of bursts" in the grid. This problem exceeds the purpose of this work and will be discussed elsewhere.

5. Results from signal simulations

To test the statistical performance of each method, for each ratio σ_1/σ_0, for each MAW and for each TOL value, 100 realizations of the signal Y(t) (eq. 1) were simulated and the boxplots of the estimated 100 burst frequencies were obtained and compared The frequency of the modulating Gaussian signal z(t) was 2.5 bursts/s, that is 50 bursts/20s (see Fig. 2, Fig. 3, Fig. 4, and Section 3.2). The case of no bursts was simulated by setting z(t) = 0 and σ_0 =1.

5.1. Results from Method ES

Table 1 shows the results obtained by applying the ES Method to 100 signal realizations (see Section 3.2) with three ratios of σ_1/σ_0 and six MAW durations. This method does not require the definition of a threshold or of a TOL value, is largely insensitive to unequal burst amplitudes and durations and even to missing bursts; it detects a "periodicity" in the burst sequence. As evident from Fig. 4, bursts can be barely detected by a human expert for $\sigma_1/\sigma_0 = 0.7$ but are detected in most of the 100 simulated signals by the ES method, for MAW ≥ 70 ms (Table 1).

Table 1. Percentage of cases of simulated bursts correctly counted by the ES method for six values of σ_1/σ_0 and six values of MAW (100 signal realizations for each case). The complement to 100 is the percentage of cases detected as "no bursts". Human counts are no longer reliable for $\sigma_1/\sigma_0 \leq 0.7$.

	MAW (ms)					
	50	60	70	80	90	100
$\sigma_1/\sigma_0 = 0.5$	18	22	22	24	26	25
$\sigma_1/\sigma_0 = 0.6$	47	55	62	70	79	82
$\sigma_1/\sigma_0 = 0.7$	65	71	82	83	96	99
$\sigma_1/\sigma_0 = 0.8$	87	91	97	98	100	100
$\sigma_1/\sigma_0 = 0.9$	98	99	99	100	100	100
$\sigma_1/\sigma_0 = 1.0$	99	100	100	100	100	100

Experimental signals often present occasionally missing, or small, bursts. In these cases, if the criteria defined in Section 3.2.1 are satisfied, the ES method provides an estimate of the frequency of the dominant periodicity; otherwise it indicates zero bursts. To investigate this point, simulations were carried out with sinusoidal modulation $z(t) = (1- \cos 2\pi f_b t)/2$ where f_b is the burst frequency.

Sinusoidal modulation was selected to reduce the effect of the peak at the second harmonic that might interfere. Results obtained from signals created with missing bursts are depicted in Fig. 5. The technique is quite robust and provides correct estimates of burst periodicity even if about 50% of the bursts are missing, as long as there are sequences of a few bursts with the proper periodicity. This result may be desirable if the global burst periodicity pattern is of interest. The burst count will be different from the counts provided by the FT and OT methods, as indicated in Fig. 5.

Method ES performs well even when only 26 bursts are present (in small groups) out of 50 in 20 s and provides the burst periodicity of 2.5 bursts/s observed in the groups of bursts. With less than 20 scattered bursts the ES method underestimates the burst frequency or does not detect bursts. The sensitivity of the method may be adjusted by changing the criterion for the identification of the "sharp isolated peak" defined in Section 3.2.1. See Section 5.3 for the case of no burst present.

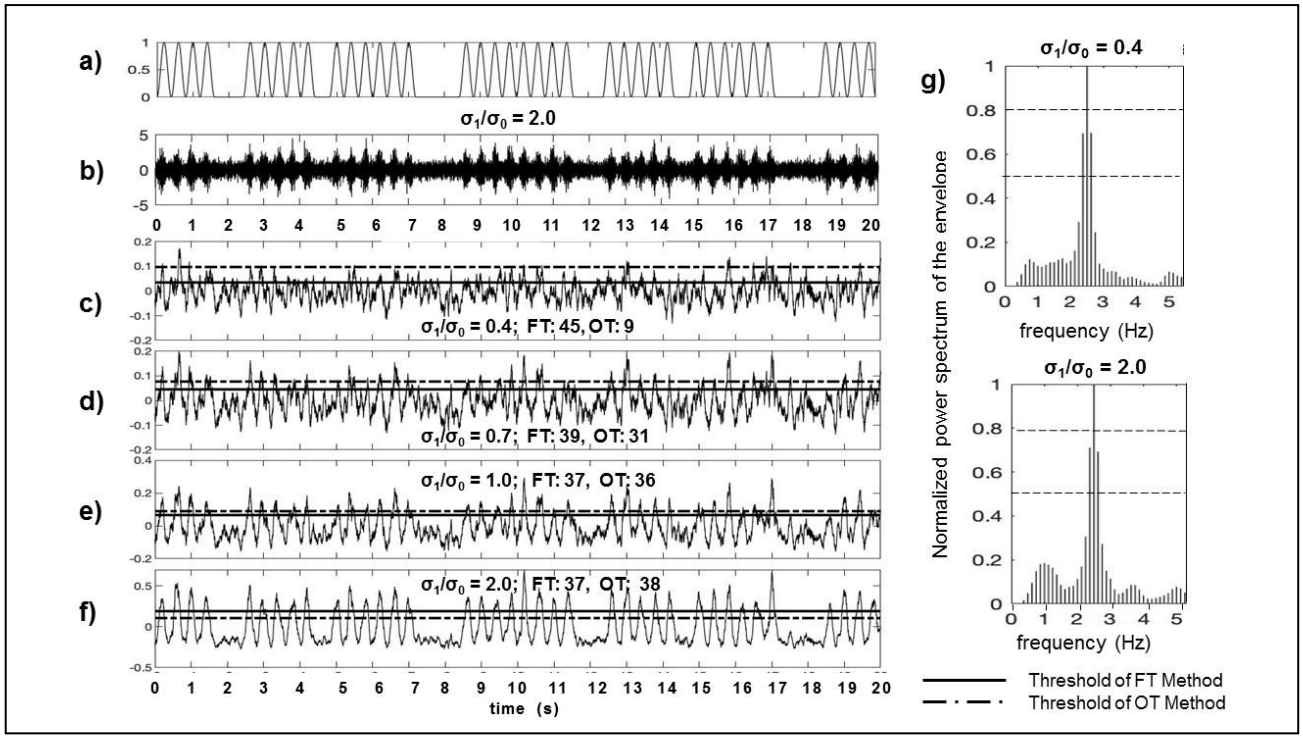

Fig. 5. Response of the three algorithms (ES, FT, OT) to a 20-s simulated signal Y(t) modulated by a sinusoidal signal z(t) =(1-cos $2\pi f_b t$)/2 with f_b =2.5 burts/s (but with only 38 bursts present) and four ratios of σ_1/σ_0. a) modulating signal z(t), b) signal Y(t) for σ_1/σ_0 = 2.0, c)-f) envelopes reconstructed by taking |Y(t)| with MAW = 80 ms, after mean removal. The FT threshold is set at the 70th percentile of the distribution of the envelope (Section 5.3) while the dot-dash line is the threshold identified by method OT (Section 5.4), g) Normalized PSD of the envelope for σ_1/σ_0=0.4 and σ_1/σ_0=2.0, clearly detecting 2.5 bursts/s (50 bursts in 20 s). The FT and OT counts are indicated in each panel. The X_0 and X_1 random signals are the same in all cases.

5.2. Results from methods FT and OT

For testing methods FT and OT, the 100 simulated Y(t) signals created to test Method ES were used with σ_1/σ_0 ratios 0.4, 0.7, 1, 2. Four threshold values, set at the 50^{th}, 60^{th}, 70^{th} and 80^{th} percentile of the distribution of the estimated envelope signal, were applied to generate a binary signal.

Three values of MAW duration (60ms, 80ms, 100 ms) were tested to empirically identify the "optimal" range of MAW. Three TOL value of 30ms, 40ms and 50ms, were applied first to the short 1's and then to the short 0's. The threshold is a critical parameter for Method FT and its best value is near the 75^{th} percentile for $\sigma_1/\sigma_0 < 1$ and near the 70^{th} percentile for $\sigma_1/\sigma_0 > 1$. See Section 5.3 for the behavior of the two methods in case of no burst. Results are shown in Fig. 6.

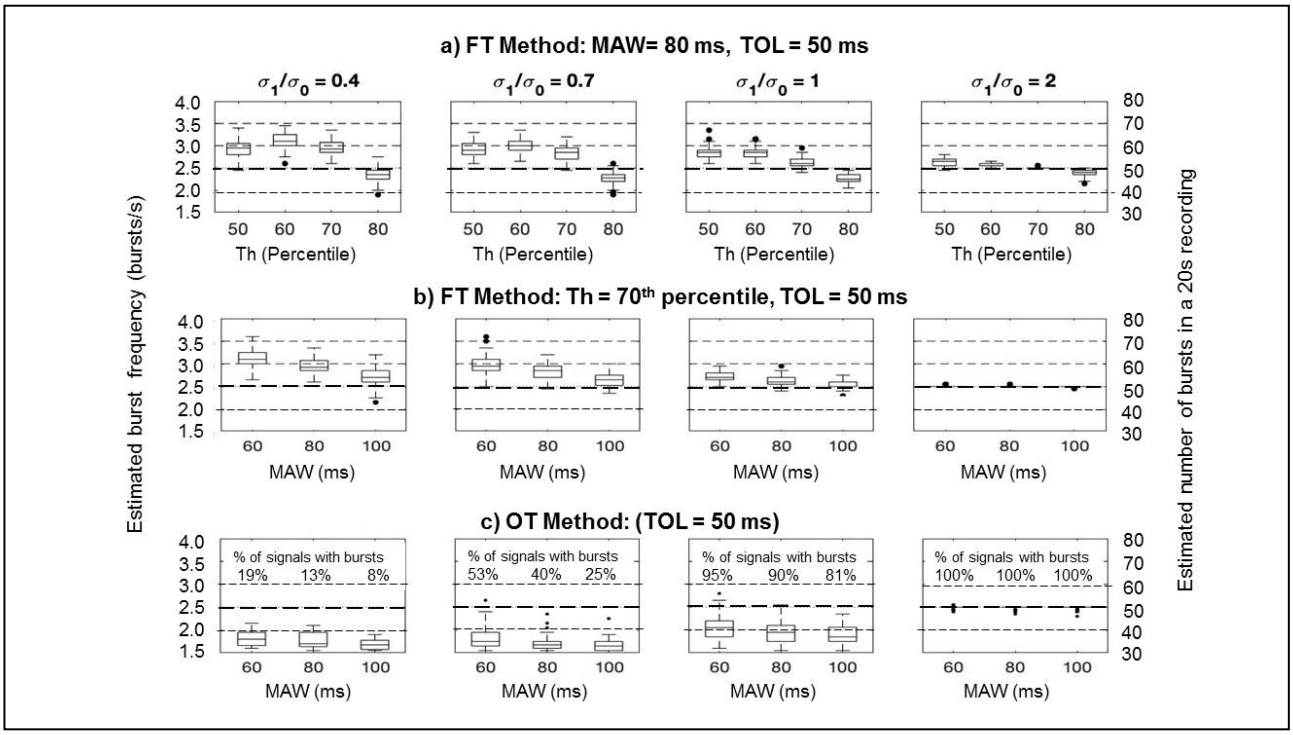

Fig. 6. Boxplots of the burst frequencies estimated from 100 signal realizations using Method FT and OT. The quartiles, range and outliers (crosses) are indicated. The correct frequency value is 2.5 bursts/s (50 bursts in 20 s). See Section 3.2.2. and 3.2.3. for details.
a) Estimated burst frequencies and counts for threshold Th in the range of the 50^{th} – 80^{th} percentile of the pdf of the envelope with Method FT (MAW 80 ms and TOL =50 ms).
b) Estimated burst frequencies and counts with Method FT for MAW = 60, 80,100 ms, TOL = 50 ms and Th=70^{th} percentile.
c) Estimated burst frequencies and counts with Method OT for MAW = 60, 80, 100 ms and TOL = 50 ms. The percentage of signals with identified bursts is indicated in each panel.

Method OT is based on the algorithm proposed by Guerrero et al [Guerrero2019] shortly described in the Appendix. The threshold is obtained from the signal itself using a Bayesian optimality

criterion. As indicated in Fig 6c and Fig. 7, acceptable burst frequency estimates are obtained for $\sigma_1/\sigma_0 > 1.5$. This method requires the setting of only two parameters (MAW and TOL).

Fig. 8 provides eight examples of envelope signals (after mean removal) obtained from signals Y(t) where z(t) is sequence of Gaussian pulses having σ = 54 ms (see Fig. 4 and Section 3.1).

Method ES provides correct results for $\sigma_1/\sigma_0 > 0.7$.

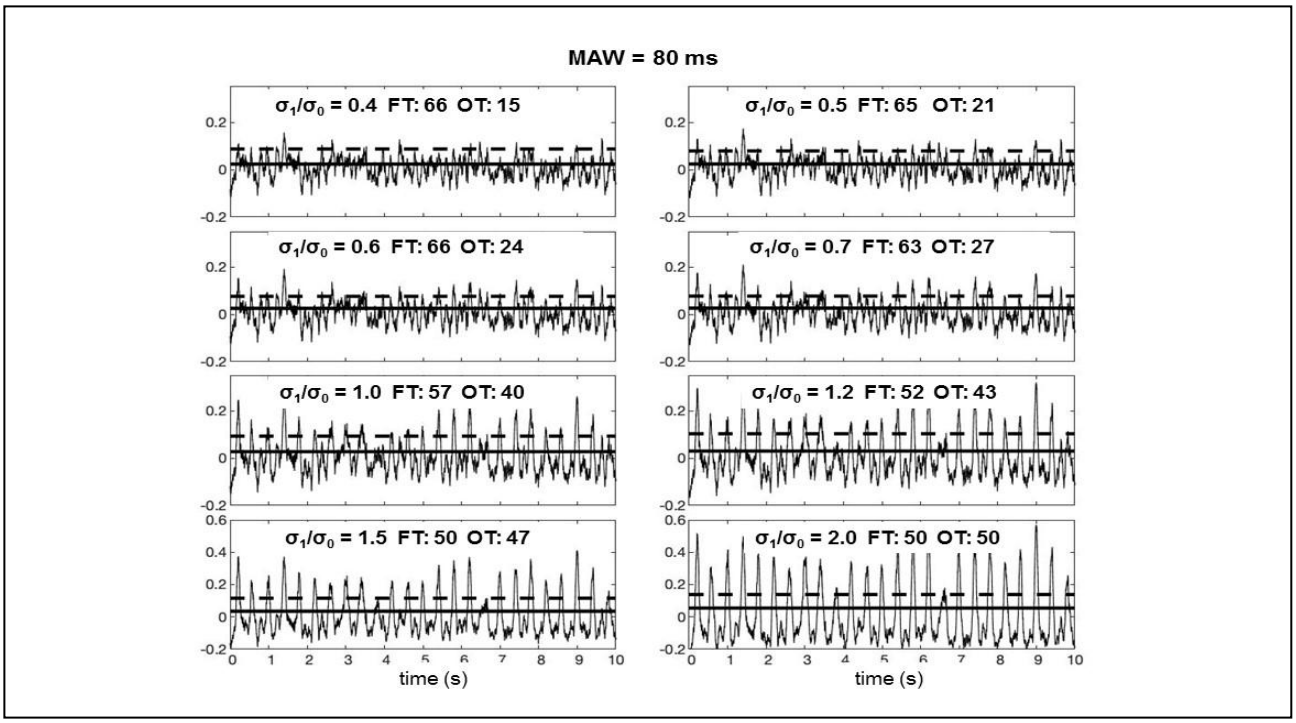

Fig. 7. Results from simulations of eight signals $Y(t) = X_0(t) + z(t) * X_1(t)$ with different ratios σ_1/σ_0 where z(t) is a sequence of 50 periodic Gaussian pulses in 20 s (see Fig. 4). For clarity, only the first 10 s are shown for each case. The fixed threshold of Method FT (solid line) and the threshold identified by Method OT (dash line) are depicted as well as the burst counts provided by the two methods over 20 s. The pattern similarities are due to the same realization of random signals X_1 and X_0 used, with proper scaling, for all cases. Burst frequency can be obtained by dividing the counts by 20.

5.3. The no burst case

A burst detection algorithm should detect no bursts when bursts are absent. This is an important requirement usually called "specificity" in the diagnostic literature and distinct from "sensitivity", the ability to detect the presence of a feature when the feature is actually there, studied in the previous sections when the feature is the presence of bursts. To test the performance of the three methods in this condition 100 Gaussian signal realizations, with zero mean, unit variance, and 20 s duration were computer generated and filtered as indicated in Section 3.1. Four values of MAW were tested (with TOLL = 50 ms for the FT and OT methods). As expected, and as

indicated in Table 2, the two threshold-based methods provide burst counts. The FT method provides burst counts in each of the 100 cases. Such counts are close the values obtained from simulated and experimental signals with clear bursts, indicating that this method is very vulnerable to false positives. The OT method provides fewer cases of false burst detection (near 45 %) and the count values are either zero or much lower than the "physiological" values observed in experimental signals. As expected, the ES method provides rare cases (1-2 %) of observed envelope "periodicity".

Table 2: Counts provided by the three methods applied to 100 20-s-long signal realizations with no bursts (100 cases with counts = 0) for four MAW values.

	MAW (ms)	Min count	Max count	Mean count	St. dev. of counts	N. of cases with counts =0
ES	70	77	77	77	0	99
	80	77	77	77	0	99
	90	0	0	0	0	100
	100	32	32	32	0	98
FT	70	47	70	61,0	1,15	0
	80	48	69	59,1	0,90	0
	90	48	66	56,9	0,79	0
	100	41	61	54,4	0,89	0
OT	70	1	43	22.6	10.34	46
	80	1	38	22.4	10.14	45
	90	1	38	22.2	9.33	45
	100	1	37	21.9	8.90	45

6. Results from experimental signals

6.1. **Burst estimation from single channel signals**

On the basis of the simulation results, a threshold equal to the 70th percentile of the distribution of the envelope signal was selected for the analysis of bursts using method FT. The values MAW = 80 ms and TOL = 50 ms were selected for both methods FT and OT. MAW = 80 ms was also selected for method ES. The criterion described in Section 3.2.1. was adopted to detect the presence/absence of bursts and their frequency with Method ES. Fig. 8 shows four examples of experimental envelope signals, the thresholds associated to Method FT and OT, the PSDs of the envelope signals, and the corresponding burst frequencies.

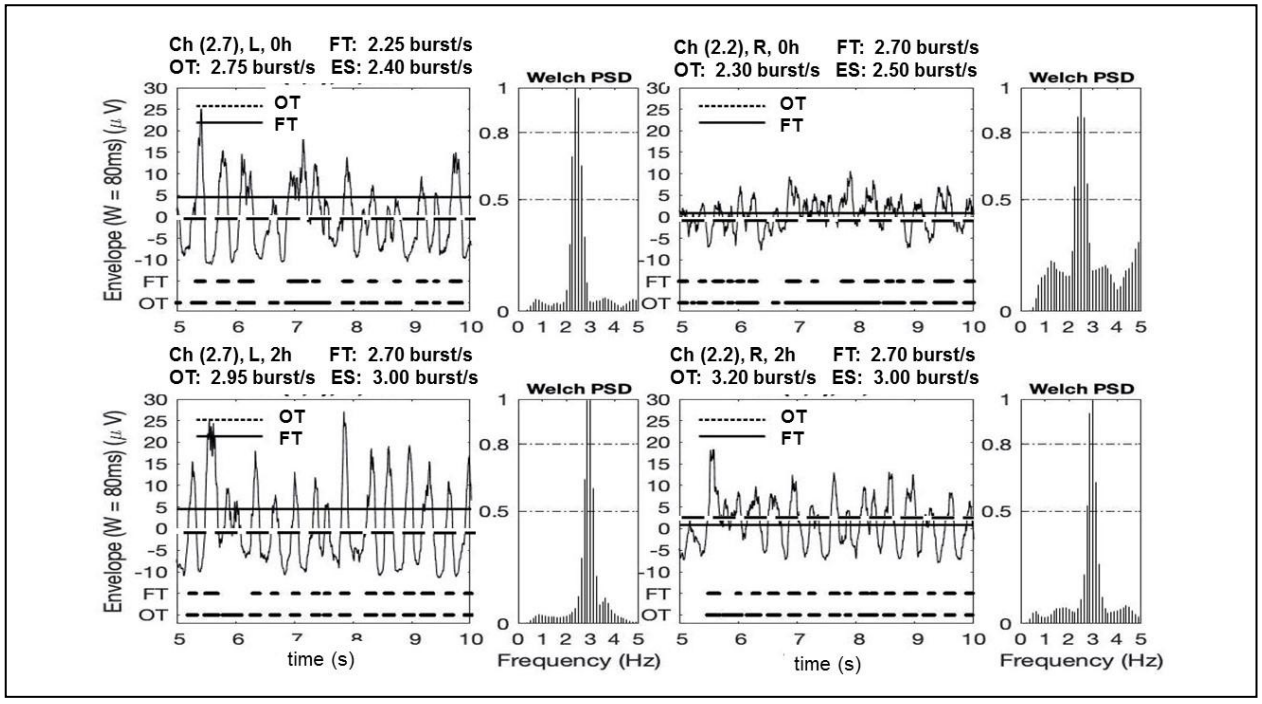

400

Fig. 8. Four examples of envelopes obtained from experimental signals detected near the spine, two on the left and two on the right side of the same subject. The mean was removed from the envelopes in order to have them centered on the zero value. The thresholds and the burst frequencies were estimated on each entire 20-s recording but only 5 s of the 20-s recordings are reported for clarity. The continuous line indicates the threshold used for the FT method (70th percentile of the pdf of the envelope signals), the dashed line indicates the estimated threshold provided by method OT. The PSDs of the envelopes are reported to the right of the corresponding signals; all four satisfy the criterion indicated in Section 3.2.1. and provide an estimate of the burst frequency. The on-off burst intervals identified by methods FT and OT are indicated at the bottom of each signal panel.
410 *MAW = 80 ms was used for the three methods and TOL = 50 ms was used for methods FT and OT. R = right side, L = left side, 0h =initial time, 2h= after 2 hours of playing.*

6.2. Burst estimation from array signals

The threshold-based methods show that presence of synchronous bursts can be observed along each column (as expected) as well as across columns of each array (across MUs and muscles). Bursts on the right and left sides appear to be synchronized, as indicated in Fig. 9 (Method FT). This phenomenon cannot be shown by the ES method.

420 Table 3 shows an example of maps of burst counts, obtained using the three methods and the human expert count (HC), from the grid of 120 SD channels on the left side of one subject at time zero. Similar results are obtained from the right side, at different times and in different subjects and will be reported elsewhere. The HC is taken as a gold standard but the burst count of each channel may

easily differ by ± 1 or ± 2 when the count is repeated twice on "poor" channels. "Poor" channels show very small bursts, similar to those simulated for $\sigma_1/\sigma_0 \leq 0.7$, and, in Table 3a, are mostly in the lower left portion of the grid, on the edge of the muscles (Fig. 1a and 1c).

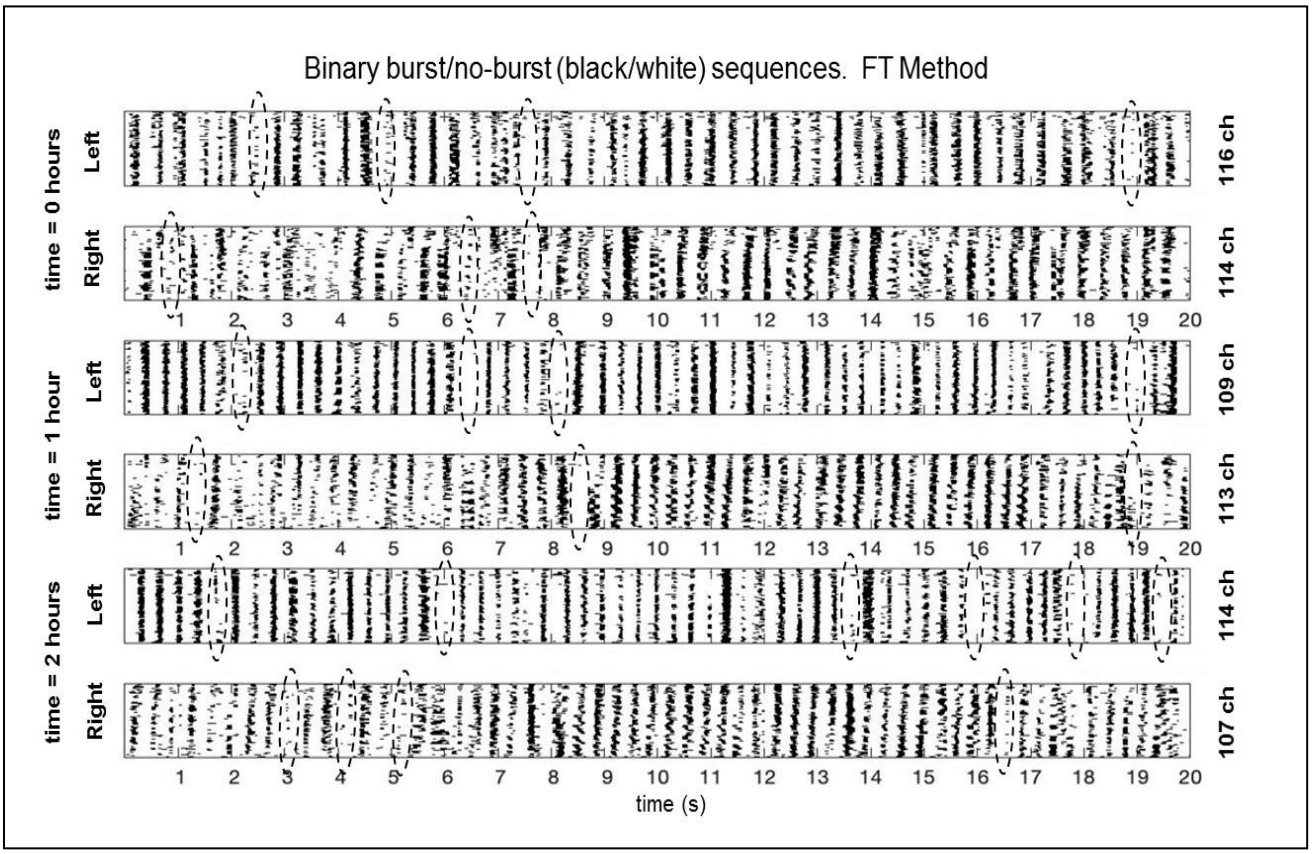

Fig. 9. Binary signals, representing bursts, obtained with Method FT after post processing. Method FT provided a 20s-long time line containing a sequence of black (envelope above threshold) and white (envelope below threshold) segments for each channel. Lines corresponding to individual channels of the same array are placed one below the other, in each panel, to show synchronized bursts on the different channels. The number of channels showing bursts identified by Method ES (out of 120) is indicated on the right for each panel. Synchronization between bursts observed within each array as well as between the right and left arrays is evident and strong. Occasional missing bursts are outlined by the dashed ellipses. Most of them are "filled in" by the ES method. R = right side, L = left side, 0h = initial time, 1h = after 1 hours of playing, 2h = after 2 hours of playing.

Table 3. Burst counts (bursts/20 s) obtained with methods ES, FT, OT and HC from each of the 120 SD sEMG channels of the left grid at time 0 hours from subject LS [Russo2019]. b) mean, standard deviation, range of counts and burst frequency of the N channels showing non-zero counts. The RMS error of the counts ($RMSE_C$) between each map and the HC is 2.42 counts between ES and HC, 3.58 between FT and HC, 9.96 between OT and HC). but highly significant distribution differences are pointed out by the Wilcoxon signed rank test that gives $p < 0.003$ for all the three comparisons (ES-HC, FT-HC, OT-HC). Pairs of channels containing one or two zeros were not included in the statistical tests. See text for furthers explanation. b/s = bursts/s.

a)

rows	ES Method (columns)								FT Method (Th = 70th percentile) (columns)								OT Method (columns)								HC (columns)							
	1	2	3	4	5	6	7	8	1	2	3	4	5	6	7	8	1	2	3	4	5	6	7	8	1	2	3	4	5	6	7	8
1	50	48	48	48	48	48	48	48	55	46	47	52	46	48	48	46	40	39	52	60	53	52	53	55	49	51	50	53	51	50	51	48
2	48	48	48	48	48	48	48	50	49	49	48	45	46	45	45	45	48	44	62	55	54	56	55	54	44	45	50	49	48	49	49	48
3	50	48	48	48	48	48	48	48	49	49	48	48	45	46	46	46	45	52	54	56	57	54	54	57	42	44	47	50	47	50	49	49
4	48	48	48	48	48	48	48	50	55	49	51	49	50	47	47	51	49	55	56	53	54	53	55	58	0	49	50	49	48	48	48	48
5	50	48	48	48	48	48	50	50	52	55	55	53	50	51	51	50	46	63	66	57	57	58	57	58	48	49	51	51	48	49	49	49
6	50	48	48	48	48	48	48	48	56	54	54	52	49	48	48	51	58	63	65	61	58	59	58	60	46	49	48	49	49	49	49	50
7	48	48	48	48	48	48	48	48	55	52	52	51	48	46	49	51	62	54	61	56	56	52	58	60	49	51	53	49	47	49	51	51
8	48	48	50	48	48	48	48	48	53	55	54	49	48	49	50	51	58	60	63	58	55	53	53	54	49	51	47	49	48	49	50	51
9	0	0	48	48	48	48	48	48	55	51	48	49	50	49	50	52	46	26	57	57	59	57	53	60	0	0	49	48	51	49	50	49
10	48	50	50	48	48	48	48	48	50	51	52	50	50	48	49	50	31	29	60	62	59	55	54	62	50	50	51	48	48	48	48	49
11	48	50	50	50	50	48	48	48	49	54	50	51	53	52	47	52	28	58	59	57	59	60	57	65	50	46	52	49	51	50	53	54
12	0	50	50	50	50	48	48	50	57	56	54	52	52	52	50	52	12	59	60	57	57	60	57	60	0	49	53	49	50	51	50	48
13	50	50	50	48	48	48	48	50	52	51	53	52	52	51	51	50	32	37	56	54	57	57	60	62	0	42	47	47	49	47	50	48
14	50	50	48	48	48	48	48	50	55	53	49	49	51	51	53	55	23	37	45	56	58	61	61	65	0	0	46	47	51	0	52	49
15	0	50	50	48	48	48	48	50	57	50	55	50	49	54	55	58	17	35	18	38	61	64	64	75	47	0	0	46	50	53	51	49

b)

N	mean ± std	range	N	mean ± std	range	N	mean ± std	range	N	mean ± std	range
116	48.5 ± 0.9	48 - 50	120	50.6 ± 3.0	45 - 58	120	53.6 ± 10.5	12 - 75	110	49.0 ± 2.1	42 - 54
Freq (b/s)	2.42 ± 0.04	2.40 - 2.50	**Freq** (b/s)	2.53 ± 0.15	2.25 - 2.90	**Freq** (b/s)	2.68 ± 0.53	0.60 -3.75	**Freq** (b/s)	2.45 ± 0.10	2.10 - 2.70
$RMSE_C$ = 2.42 burst (ES – HC)			**$RMSE_C$** = 3.58 burst (FT – HC)			**$RMSE_C$** = 9.96 burst (OT – HC)					

The methods occasionally disagree about the presence/absence of bursts. Channel pairs where at least one of the two channels have burst count = 0 are not included in the calculations $RMSE_C$.

7. Discussion and conclusions.

7.1 Discussion

At the lumbar level, the erector spinae group comprises three muscles with fibers slightly inclined with respect to the spine (Fig. 1a) [DeFoa1989]. They span a width of about 80 mm on each side of the spine and run from above T11 to below L4, that is, under the electrode array. It is therefore expected to see propagation of MUAPs along the columns of the array, as observed by Russo et al. [Russo2019]. This propagation explains the synchronization of bursts along each column of each arrays. However, marked bursts synchronization across columns of the same array, and across the right and left arrays, is evident, as depicted in Fig. 9, indicating that the CNS drives the right and the left muscles almost synchronously. This opens up a number of neurophysiological questions that will be addressed in future work.

The three methods presented for describing the quasi-periodic sEMG bursts operate on the envelope of the rectified signal and have different properties. Method ES is based on the presence of a "sharp peak" in the power spectrum of the envelope signal whose frequency reflects the "periodicity" of the bursts and is not sensitive to occasionally missing or undetectable bursts (Fig. 5 and Fig.8). This is the reason for occasional disagreement with the HC. The sensitivity of this method can be tuned by adjusting the acceptable width of the sharp peak. This method recognizes presence/absence of bursts and provides the bursts frequency estimates closest to those of a HC. Simulations indicate that a) proper length of the MAW is 80-90 ms and b) proper Th for the FT method is the 70^{th} – 75^{th} percentile of the distribution of the envelope. Longer windows smooth the envelope but reduce its amplitude, limiting the performance of methods FT and OT. The previous choice of the 50^{th} percentile [Russo2019] tends to overestimate the burst frequency (Fig. 6). The FT method does not recognize presence/absence of bursts but provides information about burst duration. Method OT automatically identifies the threshold, does not always recognize presence/absence of bursts, provides information about burst duration, and works well when bursts are evident. A good, but not critical, TOL value is 50 ms for both FT and OT.

In some cases the burst amplitude may show a trend or fluctuations either in amplitude or frequency and epochs shorter than 20 s might be more appropriate. Epochs of 5 s or 10 s would track a trend but the spectral estimates would be performed on shorter time windows and more undesirable interpolation would be required by zero-padding in the time domain. The study of burst duration will be addressed in future work as well as the study of intra and inter-subject repeatability.

7.2. Conclusions

A few preliminary analysis like that depicted in Table 3 point out that the best match with HC is provided by the ES method but the statistical distribution of the two counts is different despite the small difference between mean estimates. $RMSE_c$ values (with respect to HC) range from 2.42 burst for ES, to 3.58 bursts for FT, to 9.86 bursts for OT. This may likely be attributed, in part, to errors in human counts (e.g. separation of very close bursts or missed recognition of small ones). An important limitation of the FT and OT methods is their identification of bursts due to random local fluctuations of sEMG amplitude without burst activity (Table 2). A preliminary selection of sEMG recordings with and without burst should be implemented before applying these threshold-based methods. The ES method appears to be suitable for this purpose when the bursts are quasi-periodic.

This work provides basic tools that will allow further and more detailed investigation of sEMG bursts in ergonomic and occupational medicine for the study of posture, chairs, workstations, and various conditions (e.g. back pain, fatigue).

8. Limitations of the work and future developments

Four limitations of this work could be overcome in future investigations and could provide a more accurate comparison between methods.

1. Simulations have been performed by generating band limited white Gaussian noise band-pass filtered between 20 Hz and 400 Hz. Better simulations of the sEMG spectrum, such as the one proposed by Shwedik et al [Shwedik77] and used in the work of Guerrero [Guerrero2019], or simulations based on physiological models [Farina2001] could be more suitable. However, spectral properties of the raw signal are largely smoothed out by the low-pass filter applied to obtain the envelope and are not expected to substantially affect the results.
2. Bursts are simulated by amplitude modulating a Gaussian signal with a train of Gaussian bells and adding a second Gaussian signal, as done by Guerrero et al. [Guerrero2019]. Although sEMG signals produced by strong contraction levels are known to have a Gaussian distribution, this is not the case for signals produced by low level contractions, as in our case. A Laplacian distribution of the simulated signals might be more realistic.
3. A moving average filter was applied to the absolute value of the simulated and experimental raw signals in order to obtain the envelope. This is a frequently applied technique in sEMG processing but low-pass filtering with cut-off between 5 Hz and 10 Hz is also a common practice. Further investigations are needed to decide if either method should be preferred.
4. In a number of cases bursts appear to be present (according to the ES method) only on a portion of the grid channels. A criterion for defining global presence/absence of bursts and their frequency in the muscle(s) under a grid exceeds the purpose of this work but could be based on a majority rule or on the features of the burst map.

Further work needs to be carried out concerning the quantification of right-left synchronization by defining a synchronization index. Interesting results are expected from the decomposition of the sEMG into its constituent MUAP trains to study if the same motor units are involved, across time, in the burst generation or if they change and are rotating to compensate for fatigue [Farina2010].

References

[DeFoa1989] De Foa JL, Forrest W, Biedermann HJ.
Muscle fibre direction of longissimus, iliocostalis and multifidus: landmark-derived reference lines.
J Anat. 1989;163:243-7.

[Morasso 2011] Morasso P. 'Brute force' *vs.* 'gentle taps' in the control of unstable loads
J Physiol 589.3 (2011):459–460, doi: 10.1113/jphysiol.2010.203604

[Gawthrop2011] Gawthrop P, Loram I, Lakie M, Gollee H. Intermittent control: a computational theory of human control. Biol Cybern. 2011 Feb;104(1-2):31-51. doi: 10.1007/s00422-010-0416-4.

[Gross2002] Gross J, Timmermann L, Kujala J, Dirks M, Schmitz F, Salmelin R, Schnitzler A. The neural basis of intermittent motor control in humans. PNAS 2002; 99(4): 2299-2230,
doi: 10.1073/pnas.032682099

[Tanabe2017] Tanabe H, Fujii K, Kouzaki. Intermittent muscle activity in the feedback loop of postural control system during natural quiet standing. Sci. Rep. 2017; 7(10631),
www.nature.com/scientificreports doi: 10.1038/s41598-017-10015-8.

[Vieira 2012] Vieira TMM, Loram ID, Muceli S, Merletti R, Farina D. Recruitment of motor units in the medial gastrocnemius muscle during human quiet standing: Is recruitment intermittent? what triggers recruitment? J. of Neurophys. 2012; 107(2): 666–676, doi:
10.1152/jn.00659.2011

[Guerrero2014] Guerrero J.A., Macías-Díaz J.E. A computational method for the detection of activation/deactivation patterns in biological signals with three levels of electric intensity
Mathematical Biosciences 2014; 248: 117–127. https://doi.org/10.1016/j.mbs.2013.12.010

[Guerrero2019] Guerrero J.A., Macias-Diaz J.E.
An optimal Bayesian threshold method for onset detection in electric biosignals
Mathematical Biosciences 2019; 309: 12–22, doi: 10.1016/j.mbs.2018.12.016

[Bonato1998] Bonato P., D'Alessio T., Knaflitz M. A Statistical Method for the Measurement of Muscle Activation Intervals from Surface Myoelectric Signal During Gait
IEEE Transactions on Biomedical Engineering 1998; 45 (3): 287-299
https://doi.org/10.1109/10.661154.

[Johnson2003] Johnson TD, Elashoff RM, Harkema SJ, A Bayesian change-point analysis of electromyographic data: detecting muscle activation patterns and associated applications
Biostatistics 2003; **4** (1): 143–164, doi: 10.1093/biostatistics/4.1.143

[Ranaldi2018] Ranaldi S., De Marchis C., Conforto S., An automatic adaptive, information based algorithm for the extraction of the sEMG envelope. J. of Electrom. and Kinesiol. 2018; 48: 1-9,
doi: 10.1016/j.jelekin.2018.06.001

[Xu2013] Xu Q, Quan Y, Yang L, He J. An adaptive algorithm for the determination of the onset and offset of muscle contraction by EMG signal processing. IEEE Trans Neural Syst Rehabil Eng. 2013; 21(1): 65-73. doi: 10.1109/TNSRE.2012.2226916.

[Tenan2017] Tenan MS, Tweedell AJ, Haynes CA, Analysis of statistical and standard algorithms for detecting muscle onset with surface electromyography. PLoS ONE 2017; 12(5): e0177312. https://doi.org/10.1371/journal.pone.0177312

[Jubany2016] Jubany, J., Angulo-Barroso, R., 2016. An algorithm for detecting EMG onset/offset in trunk muscles during a reaction- stabilization test. J. Back Musculoskeletal Rehabil. 2016;29 (2): 219–230. https://doi.org/10.3233/BMR-150617.

[Yang2017] Yang, D., Zhang, H., Gu, Y., Liu, H., Accurate EMG onset detection in pathological, weak and noisy myoelectric signals. Biomed. Signal Process. Control 2017; 33: 306–315. https://doi.org/10.1016/j.bspc.2016.12.014.

[Özgünen2010] Özgünen K. T., Çelik U.,and Kurdak S., Determination of an Optimal Threshold Value for Muscle Activity Detection in EMG Analysis, J Sports Sci. Med. 2010; 9(4): 620-628. eCollection 2010

[Allison2003] Allison GT. Trunk muscle onset detection technique for EMG signals with ECG artefact. J Electromyogr Kinesiol. 2003; 13(3): 209-16. doi: 10.1016/s1050-6411(03)00019-1

[Russo2019] Russo A., Aranceta-Garza A., D'Emanuele S., Serafino F., Merletti R., HDsEMG activity of the lumbar erector spinae in violin players: comparison of two chairs. Medical Probl. of Perform. Artists, 2019; 34(4): 205-214, doi: 10.21091/mppa.2019.4034

[Merletti2016] Merletti R, Farina D. (edts) Surface Electromyography: physiology, engineering and applications, IEEE Press / J Wiley, USA, May 2016

[Merletti2019] Merletti R., Muceli S., Tutorial. Tutorial. Surface EMG detection in space and time: Best practices. Journal of Electromyography and Kinesiology 2019; 59: 102363 (free article on line) doi: 10.1016/j.jelekin.2019.102363

[Nazarpour2013] Nazarpour K., Al-Timemy A., Bugmann G., Jackson A., A note on the probability distribution function of the surface electromyogram signal. Brain Res. Bulletin, 2013; 90: 88-91, doi: 10.1016/j.brainresbull.2012.09.012

[Shwedik1977] Shwedyk, E., R. Balasubramanian and R. Scott, "A non-stationary model of the electromyogram" *IEEE Trans. B.M.E.* 1977; 24: 417-424. doi: 10.1109/TBME.1977.326175

[Mewett2004] Mewett, D. T., Reynolds, K. J., and Nazeran, H., Reducing power line interference in digitised electromyogram recordings by spectrum interpolation. Medical and Biological Engineering and Computing 2004; 42 (4): 524-531. doi: 10.1007/BF02350994.

[Leske2019] Leske S, Dalal S.S. Reducing power line noise in EEG and MEG data via spectrum interpolation. Neuroimage; 2019; 189: 763-776. doi: 10.1016/j.neuroimage.2019.01.026

[Farina2001] Farina D., Merletti R., A novel approach for precise simulation of the EMG signal detected by surface electrodes, IEEE Trans. on Biomed. Eng., 2001; 48: 637-646, doi: 10.1109/10.923782

[Farina2010] Farina D, Holobar A, Merletti R, Enoka RM. Decoding the neural drive to muscles from the surface electromyogram. Clin Neurophysiol. 2010;1 21(10): 1616-23. doi: 10.1016/j.clinph.2009.10.040.

Appendix

Appendix - Brief description of the method proposed by Guerrero and Macias-Diaz.

The starting assumption of the method proposed in [Guerrero2019] is that each value x_i of the signal is a realization of a continuous r.v. X_i with mean 0, for each $i = 1, \dots, n$. Each x_i belongs either to an activity phase or a silence phase, so that we can consider a Bernoulli r.v. Θ, the silence/activation r.v., such that

$$\theta_j = \begin{cases} 1, & \text{if the sample } x_j \text{ belongs to the activity phase} \\ 0, & \text{otherwise,} \end{cases} \qquad 1)$$

where θ_j is a realization Θ. The r.v. X which describes the signal samples is then modelled as a new r.v. which is a mixture of two Gaussian r.v.'s $X|(\Theta = j) \sim N(0, \sigma_j^2)$, $j = 0, 1$ as follows

$$X = \lambda \cdot X|(\Theta = 0) + (1 - \lambda) \cdot X|(\Theta = 1), \qquad \lambda \in [0,1]. \qquad 2)$$

In general, given a random variable Z, the so-called *Optimal Bayesian Classifier* (OBC) is a procedure which assigns an observation z_j to the active phase or to the silence phase according to the rule

$$\hat{\theta}_j(z_j) = \begin{cases} 1, & if\ P(Z = z_j|\Theta = 1) \cdot P(\Theta = 1) > P(Z = z_j|\Theta = 0)P(\Theta = 0) \\ 0, & otherwise. \end{cases} \qquad 3)$$

The previous expression assumes a convenient form for Gaussian r.v. $X|(\Theta = j) \sim N(0, \sigma_j^2)$, $j = 0$. In this case it can be shown that the OBC is given by the disequality

$$\frac{x^2}{\sigma_0^2} - \frac{x^2}{\sigma_1^2} > 2\, log\, \frac{P(\Theta=0)\cdot\sigma_1^2}{P(\Theta=1)\cdot\sigma_0^2} \qquad 4)$$

called the *Gaussian classifier*. By imposing the equality and solving for x, just the only acceptable value is the searched threshold. It is important to notice that Guerrero's method applies the Gaussian classifier not to the r.v. X, but to a Gaussian r.v. used to approximate the moving average $\bar{Y}$ of the signal $Y = |X|$.
The expression of the threshold t_{OBC} is quite complex and it is not reported in this summary.

The main steps of the algorithm are:

Step 1. Estimate the parameters λ, σ_0, σ_1 through a classical *Expectation Maximization* (EM) algorithm for a mixture of two Gaussian random variables.

Step 2. Compute the moving average $\bar{Y}$ of the absolute value of the signal. Using the Central Limit Theorem, the distribution of the mean values above can be approximated using a normal distribution for sufficiently large sample sizes.

Step 3. Apply the optimal Bayesian classifier with $Z = \bar{Y}$, $\hat{\lambda}$ estimate of $P(\Theta = 0)$ and obtain a threshold t_{OBC}.

Step 4. Construct the silence/activation process, where activation means $\bar{Y} > t_{OBC}$.

Step 5. Post-processing by using the *morphological operators* of opening and closure: apply a closure operation followed by an opening operation on the estimated silence/activation process in Step 4.

***Declaration of Interest Statement**

Declaration of interests

☒ The authors declare that they have no known competing financial interests or personal relationships that could have appeared to influence the work reported in this paper.

☐The authors declare the following financial interests/personal relationships which may be considered as potential competing interests: